Chemical Science

EDGE ARTICLE

Check for updates

Pore closure in zeolitic imidazolate frameworks under mechanical pressure†

Sebastian Henke, [*a] Michael T. Wharmby, [‡b] Gregor Kieslich, [c] Inke Hante,[d] Andreas Schneemann, [§c] Yue Wu, [e] Dominik Daisenberger[b] and Anthony K. Cheetham [e]

We investigate the pressure-dependent mechanical behaviour of the zeolitic imidazolate framework ZIF-4 (M(im)$_2$; M^{2+} = Co^{2+} or Zn^{2+}, im$^-$ = imidazolate) with high pressure, synchrotron powder X-ray diffraction and mercury intrusion measurements. A displacive phase transition from a highly compressible open pore (**op**) phase with continuous porosity (space group *Pbca*, bulk modulus ∼1.4 GPa) to a closed pore (**cp**) phase with inaccessible porosity (space group *P2$_1$/c*, bulk modulus ∼3.3–4.9 GPa) is triggered by the application of mechanical pressure. Over the course of the transitions, both ZIF-4 materials contract by about 20% in volume. However, the threshold pressure, the reversibility and the immediate repeatability of the phase transition depend on the metal cation. ZIF-4(Zn) undergoes the **op–cp** phase transition at a hydrostatic mechanical pressure of only 28 MPa, while ZIF-4(Co) requires about 50 MPa to initiate the transition. Interestingly, ZIF-4(Co) fully returns to the **op** phase after decompression, whereas ZIF-4(Zn) remains in the **cp** phase after pressure release and requires subsequent heating to switch back to the **op** phase. These variations in high pressure behaviour can be rationalised on the basis of the different electron configurations of the respective M^{2+} ions (3d^{10} for Zn^{2+} and 3d^7 for Co^{2+}). Our results present the first examples of **op–cp** phase transitions (*i.e.* breathing transitions) of ZIFs driven by mechanical pressure and suggest potential applications of these functional materials as shock absorbers, nanodampers, or in mechanocalorics.

Introduction

Flexible metal–organic frameworks (MOFs) have attracted considerable attention in recent years. Their unique responsive properties suggest applications in gas storage and separations, chemical sensing, catalysis, and targeted drug release.[1–4] Some flexible MOFs show displacive structural transitions in response

ªAnorganische Chemie, Fakultät für Chemie & Chemische Biologie, Technische Universität Dortmund, Otto-Hahn-Str. 6, 44227 Dortmund, Germany. E-mail: sebastian.henke@tu-dortmund.de

ᵇDiamond Light Source Ltd., Harwell Science & Innovation Campus, Didcot, Oxfordshire, OX11 0DE, UK

ᶜLehrstuhl für Anorganische und Metallorganische Chemie, Technische Universität München, Lichtenbergstr. 4, 85748 Garching, Germany

ᵈLehrstuhl für Anorganische Chemie II, Fakultät für Chemie & Biochemie, Ruhr-Universität Bochum, Universitätsstraße 150, 44801 Bochum, Germany

ᵉDepartment of Materials Science and Metallurgy, University of Cambridge, 27 Charles Babbage Road, Cambridge, CB3 0FS, UK

† Electronic supplementary information (ESI) available: Experimental details; synthetic procedures; supplementary data analyses; additional PXRD, thermal and elemental analyses as well as IR and ¹H NMR spectroscopy data. See DOI: 10.1039/c7sc04952h

‡ Present address: Deutsches Elektronen-Synchrotron (DESY), Notkestr. 85, 22607 Hamburg, Germany.

§ Present address: Sandia National Laboratories, Livermore, CA 94551-0969, USA.

to external stimuli, particularly the sorption of guest molecules.[1,5–7] Such materials can maintain their intra-framework connectivity while reversibly switching between an open, or large pore form, and a narrow, or closed pore form. The most prominent example from this class of materials is MIL-53 (MIL = Matériaux de l'Institut Lavoisier; M(OH)(bdc); bdc^{2-} = 1,4-benzenedicarboxylate), which shows a very large breathing effect upon gas adsorption (*e.g.* CO$_2$) and can be prepared with a variety of different metal ions (M^{3+} = Al^{3+}, Cr^{3+}, *etc.*).[5–8]

The guest-responsive structural flexibility of several MOFs has been thoroughly investigated and is well documented. The intrinsic structural response of such flexible frameworks to mechanical pressure, however, is relatively unexplored.[9–17] This is surprising because flexible MOFs with pressure driven phase transitions are not only of interest for applications as shock absorbers, nanodampers, and supramolecular nanosprings, but might also lead to applications in mechanocalorics.[18–25]

To the best of our knowledge, examples of breathing phase transitions¶ of MOFs in response to extrinsic mechanical pressure have only been reported for materials of the MIL-53/MIL-47 family (MIL-47 = M(O)(bdc); M^{4+} = V^{4+}).[20–28] All of these frameworks exhibit a winerack-like structure composed of infinite metal-hydroxide or metal-oxide chains, which are crosslinked by linear dicarboxylates (*e.g.* bdc^{2-} or fumarate) to

generate lozenge-shaped channels (**sra** topology). Under the influence of mechanical pressure the large pore phase of these frameworks transforms to a closed pore phase, whereby the lozenge-shaped channels contract, resulting in a highly anisotropic structural change – under pressure, the long diagonals of the channels expand, while the short diagonals contract.

Here, we report on the high pressure structural behaviour of zeolitic imidazolate frameworks (ZIFs) of the ZIF-4 family and describe an almost isotropic, displacive structural transition under mechanical pressure. ZIF-4(Zn) (**1**, $Zn(im)_2$ with im^- = imidazolate) is a microporous MOF composed of ZnN_4 tetrahedra interconnected by im^- linkers in the four-connected **cag** topology.[29,30] **1** features a number of unusual properties: it transforms into an amorphous state when heated to about 300 °C and then converts to a non-porous phase with the **zni** topology on further heating; it can also be melted at temperatures of about 600 °C, and quenched to form ZIF glasses.[31–36]

Recently, we reported that **1** also undergoes a reversible phase transition at lower temperatures. The open pore (**op**) phase of **1** transforms to a closed pore (**cp**) phase upon cooling the material below 140 K under vacuum (Fig. 1).[37] This **cp** phase features the same topology (**cag**) and connectivity as the original **op** phase; however, the unit cell contracts almost isotropically by about 23%. In this breathing process, all im^- linkers in the material undergo a concerted rotation, which results in a 3D inward folding of the framework, leading to a drastic reduction of the pore volume (from 39% to 9% of the crystal volume, see ESI†). The small pores remaining in the **cp** phase are isolated and hence inaccessible to any guest molecule. The thermodynamic driving force for the phase transition is the higher enthalpic stability of the **cp** phase, which arises from attractive dispersion interactions between the molecular building units, which move closer to each other in the **cp** phase.[37] At higher temperature the **op** phase is stabilised by vibrational entropy.

Encouraged by our previous findings, we have now investigated the high pressure behaviour of **1** as well as its isostructural cobalt-based derivative ZIF-4(Co)[38] ($Co(im)_2$, **2**) via high pressure, synchrotron powder X-ray diffraction and

mercury intrusion experiments. Breathing phase transitions triggered by comparatively low mechanical pressures are apparent for both ZIF materials, extending the family of MOFs, which show mechano-switching behaviour, to ZIFs.

Results and discussion

To investigate the structural behaviour of **1** and **2** as a function of mechanical pressure, we conducted high pressure powder X-ray diffraction (HP-PXRD). The experiments were performed at beamline I15, Diamond Light Source (Oxon., UK) using a monochromatic X-ray beam with a wavelength of 0.41334 Å and membrane diamond anvil cells (mDACs) for the high pressure environment. Prior to the experiment, the ZIF samples were thoroughly evacuated at 130 °C under dynamic vacuum to ensure complete activation. Absence of any adsorbed guest molecules was verified by elemental and thermogravimetric analyses as well as IR spectroscopy of the powder samples (Fig. S15 and S16†). In addition, ^{1}H NMR spectroscopy was carried out on evacuated samples digested in DMSO-d_6/DCl/D_2O. Residual organic solvents could not be detected by ^{1}H NMR spectroscopy (Fig. S17 and S18†). For HP-PXRD measurements, the samples were loaded into mDACs under an inert atmosphere inside an Ar-filled glove box with an alkali halide internal pressure standard (NaCl for **1** and KBr for **2**). Fluorinert FC-70, which is too large to penetrate into the micropores of **1** and **2**, was used as a pressure transmitting fluid. Diffraction data were collected from ambient pressure up to about 2–3 GPa. The HP-PXRD patterns were analysed by structure-less Pawley refinement (see ESI† for further details).[39]

1 and **2** are isostructural at ambient pressure and the diffraction patterns are in accordance with the **op** phase of **1** reported previously (orthorhombic, $Pbca$, $a = 15.50051(15)$ Å, $b = 15.52013(14)$ Å, $c = 18.05823(17)$ Å, $V = 4344.27(7)$ Å^3; see Fig. 2).[37] Upon increasing hydrostatic pressure, **1** rapidly undergoes a phase transition to a new phase, which goes to completion by about 75 MPa (Fig. 2 and S4†). The corresponding PXRD pattern is similar, but not identical, to the diffraction pattern of the established low temperature **cp** phase of **1** (orthorhombic $Pbca$, $a = 14.26686(9)$ Å, $b = 14.28427(8)$ Å, $c = 16.41270(11)$ Å, $V = 3344.77(4)$ Å^3).[37] The pattern recorded at ~75 MPa is more complex and features additional Bragg peaks, which led us to the conclusion that the high pressure **cp** phase of **1** differs from the established low temperature **cp** phase. Additional Bragg peaks in the pattern suggest a distortion of the structure from the orthorhombic to a monoclinic lattice. We tried to fit the PXRD pattern in monoclinic settings based on the most symmetric monoclinic subgroups (space groups $P2_1/b11$, $P12_1/c1$ or $P112_1/a$) of the original orthorhombic structure (space group $Pbca$).‖ The best fit to the experimental data was found for the monoclinic setting in $P12_1/c1$, with lattice parameters similar to the ones for the low temperature **cp** phase (Table 1 and Fig. 3). Hence, we conclude that the high pressure **cp** phase of **1** is indeed similar to the low temperature **cp** phase, but it involves a small shear element as indicated by a β angle of 91.55(3)°. It is noteworthy that the unit cell volume of the monoclinic high pressure **cp** phase of **1** is slightly larger ($V =$
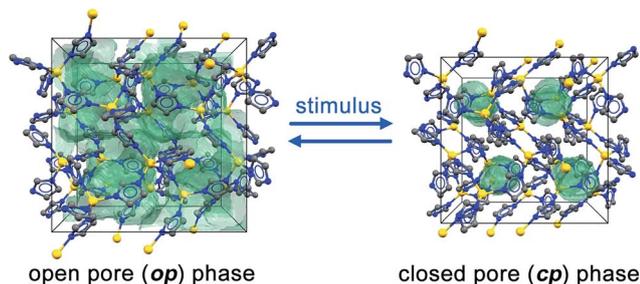

Fig. 1 View on a unit cell of the crystal structure of desolvated ZIF-4(Zn) (**1**) along the crystallographic c axis. At room temperature the framework exhibits an open pore (**op**) phase exhibiting continuous porosity and at temperatures below 140 K the material features a closed pore (**cp**) phase with very small and inaccessible pores. C, N and Zn atoms are shown in grey, blue and yellow, respectively. The void surface is shown in green. Both structures are drawn to the same scale.
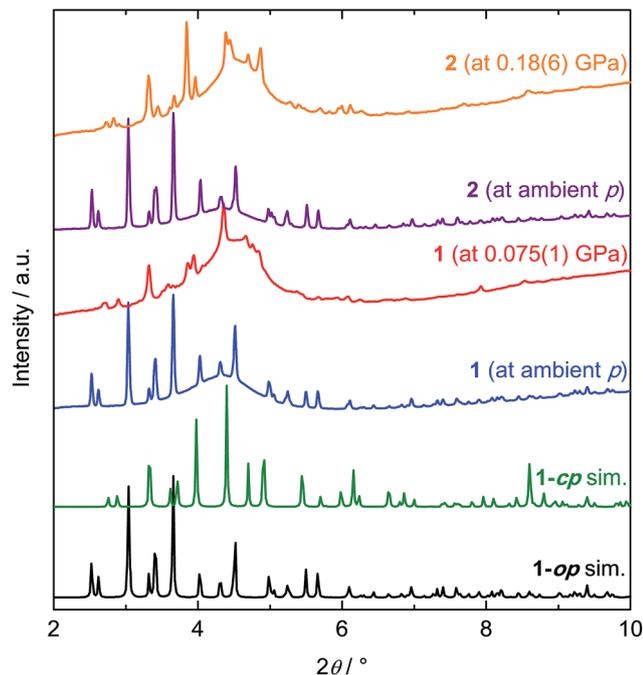
Fig. 2 Collection of PXRD patterns of **1** and **2** recorded at ambient pressure (blue and purple) and at high pressure (orange and red). Diffractograms were recorded using a monochromatic X-ray beam with $\lambda = 0.41334$ Å. Simulated diffraction patterns for the room temperature **op** and low temperature **cp** phases of **1** (taken from ref. 37) are shown for comparison (black and green). The broad hump in the background of the experimental patterns is attributed to diffuse scattering from the pressure transmitting fluid. The patterns have been normalised and offset vertically for clarity.

Table 1 Crystallographic data of the ambient pressure (**op**) and high pressure (**cp**) phases of **1** and **2** as determined from PXRD data

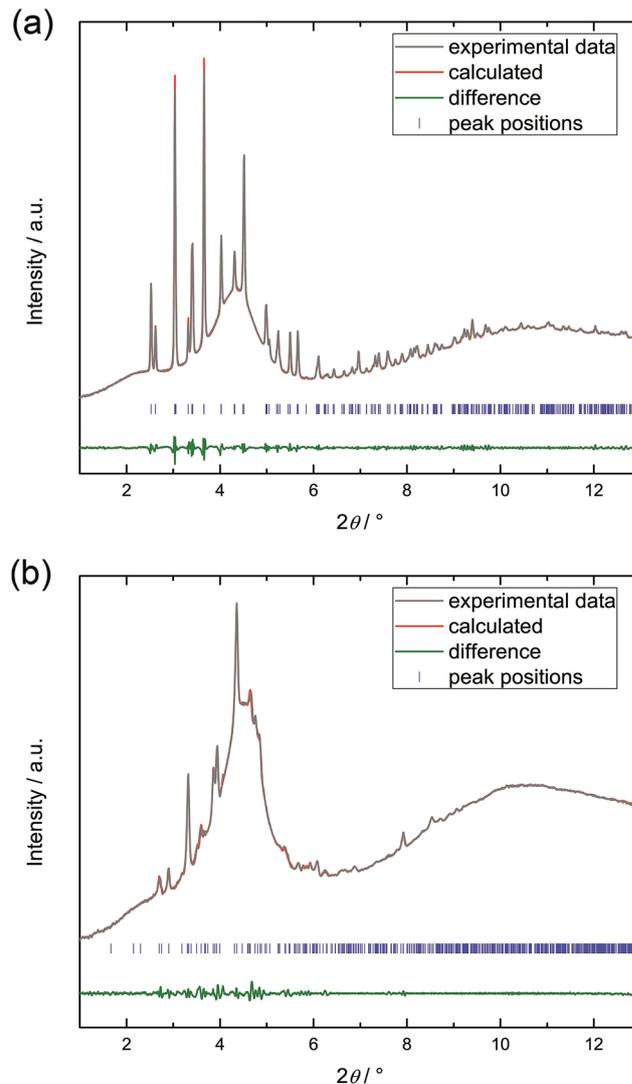| Compound	1-op	1-cp	2-op	2-cp
p/GPa	$\sim 10^{-4}$	0.075(10)	$\sim 10^{-4}$	0.18(6)
a/Å	15.502(3)	14.235(12)	15.440(2)	13.981(9)
b/Å	15.524(2)	14.874(18)	15.5102(18)	15.045(13)
c/Å	18.079(3)	16.33(2)	18.082(2)	16.636(15)
α/°	90	90	90	90
β/°	90	91.55(3)	90	90.761(11)
γ/°	90	90	90	90
V/Å^3	4350.9(13)	3457(7)	4330.1(9)	3499(5)
S.G.	$Pbca$	$P2_1/c$	$Pbca$	$P2_1/c$

Fig. 3 Pawley fit to the diffraction patterns of compound **1** recorded at ambient pressure (a) and at 0.075(10) GPa (b). Diffractograms were recorded using a monochromatic X-ray beam with $\lambda = 0.41334$ Å. The very broad peak (centered at ~ 4.4°) underneath the Bragg peaks is attributed to the diffuse scattering from the pressure transmitting fluid FC-70. Crystallographic parameters are listed in Table 1.

3457(7) Å^3) than the unit cell volume of the orthorhombic low temperature **cp** phase ($V = 3345(7)$ Å^3), which might originate from higher vibrational entropy at ambient temperature (HP-PXRD experiment) compared to at 80 K (variable temperature PXRD experiment).[40] Nevertheless, the unit cell volume reduces by about 21% over the pressure-induced phase transition.

Further increasing the mechanical pressure results in a monotonic contraction of the **cp** phase, which is apparent by the shifting of the Bragg peaks to higher 2θ angles (Fig. S4†). In this process the reflections also get much broader, finally resulting in a largely amorphised material at ~ 1 GPa. We note that the amorphisation of **1** seems to be irreversible since the

largely amorphised material does not recover its original crystalline state after returning to ambient pressure (see ESI†). This observation deviates from previous findings by Bennett *et al.*, who reported reversible amorphisation of **1** under mechanical pressure.[32] The reason for this difference may be that we compressed **1** to a maximum pressure of about 2 GPa in the HP-PXRD experiment, while Bennett *et al.* compressed the material only to about 1 GPa. The higher maximum pressure of our experiment may result in irreversible structure collapse, while the amorphisation is reversible if a pressure of 1 GPa is not exceeded.

Also in contrast to our findings, Bennett *et al.* did not observe the **op**–**cp** phase transition of **1** in their previous HP-PXRD study.[32] In their experiment the material remained in the **op** phase before amorphisation. The origin of the different phase

behaviour in the previous study might be either incomplete sample evacuation or adsorption of moisture from the atmosphere during sample preparation, both of which could impede the observation of the **op**–**cp** transition. We have already shown that, in contrast to guest-free **1**, DMF-containing **1** (**op** form) does not transform to the **cp** form upon cooling to cryogenic temperatures.[37] It therefore seems natural that the presence of even small amounts of guests could also prevent the **op**–**cp** transition under the stimulus of mechanical pressure (see ESI† for further details).

As anticipated, the cobalt-derivative **2** behaves similarly to **1**, transforming from the **op** phase to a **cp** phase under the influence of mechanical pressure (Fig. 2 and S5†). However, the pressure required to complete the transition is significantly higher (∼180 MPa). The pattern of the high pressure phase of **2** is also similar to the reference pattern of the low temperature **cp** phase of **1**, but can again only be fitted with a monoclinic unit cell in the subgroup $P2_1/c$ (see ESI† for details). The unit cell volume of **2** decreases by ∼19% at the **op**–**cp** transition. Increasing the mechanical pressure further leads to significant peak broadening and finally an irreversible transformation to a largely amorphous material at pressures in the range from 1–3 GPa (Fig. S5†). Table 1 presents the crystallographic data of the **op** and **cp** phases as determined by structure-less Pawley refinement for both compounds.

In order to obtain more information about the unusual **op**–**cp** phase transitions of both ZIF-4 derivatives in the pressure region below 200 MPa, mercury intrusion experiments were carried out. Mercury is a non-wetting liquid that cannot penetrate into micropores and acts as a hydrostatic pressure transmitting fluid. Hence, mercury intrusion experiments are ideally suited for the investigation of pressure-driven breathing transitions in microporous solids, resulting in an abrupt, large contraction.[20–26] Sharp steps in the intrusion curve can be directly assigned to phase transitions involving a density change (*i.e.* volume change) of the material under study. Advantageously, in the lower pressure range (1–200 MPa), which is of interest here, mercury intrusion experiments allow a significantly better pressure resolution than HP-PXRD experiments.

The mercury intrusion experiments were performed on freshly activated and finely ground powders of **1** and **2** in the pressure range from 10^{-3} to about 210 MPa (Fig. 4). Samples for these experiments were prepared in an Ar-filled glove box to prevent any adsorption of moisture in the guest-free ZIFs. Up to a pressure of about 1 MPa, mercury intrusion is associated with filling of the inter-particle voids of the loose crystalline powder. Beyond this point, the ZIF microcrystals are totally surrounded by mercury and increasing pressure is then applied hydrostatically to the sample.

A sharp step in the mercury intrusion curve of **1** is visible at a surprisingly low pressure of about 28 MPa. This step cannot be attributed to the ingress of mercury into the compound's pores, since according to the Washburn equation,[41] the step would indicate an effective pore diameter (*d*) of 40–50 nm (see ESI†). The pores of **1**, however, lie well within the microporous range (*d* < 2 nm). The measured volume change ΔV_{meas} at the step of
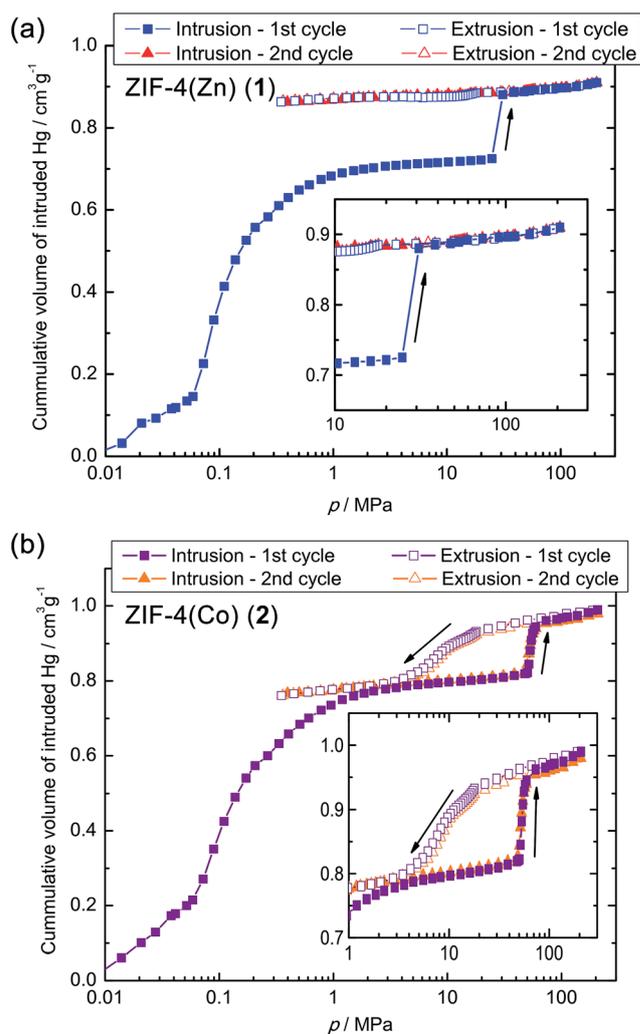

Fig. 4 Mercury intrusion–extrusion curves recorded for **1** (a) and **2** (b) at room temperature. The insets reveal a closer look on the data in the region of the **op**–**cp** phase transition, which is irreversible for **1** and reversible for **2**. Lines represent a guide to the eye only. Data have been corrected by a blank measurement. N.B. Although data were measured from 10^{-3} MPa, for clarity, only the range 10^{-2} to 210 MPa is shown.

the intrusion curve is directly proportional to the decrease in unit cell volume or the increase in sample density at the phase transition. ΔV_{meas} amounts to 0.16 cm³ g⁻¹ for **1**, which is close to the value expected for the **op**–**cp** phase transition (ΔV_{calc} = 0.169 cm³ g⁻¹; based on the change in unit cell volume determined from HP-PXRD). Hence, the prominent step in the intrusion curve can directly be ascribed to the **op**–**cp** phase transition of **1**. Noticeably, the subsequent mercury extrusion branch does not show any steps, which indicates that the **op**–**cp** phase transition is irreversible and that **1** remains in the contracted **cp** phase upon decompression. Consequently, a successive second intrusion–extrusion cycle does not show any steps associated with a phase transition.

Noticeably, the threshold pressure for the **op**–**cp** transition, indicated by the mercury intrusion curve (∼28 MPa), is significantly lower than that expected on the basis of the HP-PXRD

experiment (phase transition completed at ~75 MPa). This variation most likely originates from the different pressure transmitting medium (FC-70 vs. mercury) used in the complementary experiments (HP-PXRD vs. mercury intrusion). Large variations of the threshold pressure as a function of the pressure transmitting fluid (i.e. silicone oil vs. mercury) were also observed for the large pore to closed pore phase transitions of MIL-53-type materials.[23,24,26] For these materials, the use of silicone oil as pressure transmitting fluid resulted in a much higher threshold pressure compared to the use of mercury. This phenomenon was explained by a partial penetration of the chain ends of the silicone oil molecules into the pore opening of the MIL-53-type materials. In our HP-PXRD experiments we used Fluorinert FC-70 as pressure transmitting fluid. Similar to silicone oil, FC-70 might also partially penetrate the pore apertures of the microporous ZIF-4(M) compounds, which results in a shift of the **op–cp** transition to higher pressures compared to the use of mercury. Since mercury is a non-wetting fluid, however, the mercury intrusion data are expected to yield information on the intrinsic thermodynamic behaviour of the microporous material under study.

For reasons of comparison to other mechano-switchable MOFs (i.e. MIL-53/MIL-47-type compounds) we calculated the work (W_{trans}) done on the system during the **op–cp** phase transition on the basis of the mercury intrusion curves (see ESI† for details).** W_{trans} amounts to only ~4.4 J g^{-1} for compound **1**. Highlighting the pronounced flexibility of **1**, this value is slightly lower than the work computed for the highly flexible MIL-53(Al) (~6.6 J g^{-1}) and significantly lower than the work calculated for other MIL-53 derivatives (~14 J g^{-1} for MIL-53(Cr) and ~33 J g^{-1} for MIL-47(V); all values were computed on the basis of mercury intrusion data).[21,22,28]

Interestingly, **2** shows a different behaviour. Again a sharp step for the **op–cp** transition is apparent in the intrusion curve (Fig. 4), but, at a higher pressure of about 50 MPa (compared to 28 MPa for **1**). This pressure would correlate with an effective pore diameter of about 20 nm, which again cannot be attributed to a filling of the micropores present in **2** (see ESI†). The volume change ΔV_{meas} at the step of the intrusion curve amounts to 0.15 cm^3 g^{-1}, which again is in good agreement with the value expected for the **op–cp** phase transition ($\Delta V_{calc} = 0.162$ cm^3 g^{-1}; based on the change in unit cell volume determined from HP-PXRD). W_{trans} is ~7.3 J g^{-1} (see ESI†), which is almost twice as large as for **1** due to the significantly higher phase transition pressure of **2**. Surprisingly, compound **2** undergoes the inverse **cp–op** phase transition at pressures below 20 MPa, which is apparent as a shallow but distinct step during extrusion. The inverse transition is complete at a rather low pressure of only about 4 MPa, which gives rise to a very large hysteresis (width ~46 MPa). However, the fact that the entire volume change associated with the transition is reversible demonstrates that the phase transition is indeed completely reversible for **2**. A successive intrusion–extrusion cycle further underlines the reversibility of the **op–cp** transition of **2** under the conditions of the mercury intrusion experiment. The second cycle is virtually identical to the first cycle, except for the interparticle penetration at low pressures. A hysteretic phase behaviour as a function of an external variable (e.g. mechanical pressure, gas

pressure, temperature) is typical for such kind of flexible MOFs and has also been observed for mechanical pressure-driven structural changes of the carboxylate-based MIL-53(Cr) and MIL-47(V) materials.[20,21] Taking into account the results of the mercury intrusion and the HP-PXRD experiments, we can conclude that the **op–cp** phase transition of **2** is reversible at least if the maximum pressure is limited to about 210 MPa. At a certain threshold pressure the compound amorphises and if a pressure of about 2–3 GPa is achieved (as in the HP-PXRD experiment), this amorphisation is irreversible.

On the basis of linear fits to the mercury intrusion data, the bulk moduli (K) of the **op** and **cp** phases of **1** and **2** can be estimated (see ESI†). We found very low bulk moduli for the **op** phases of both materials ($K = 1.42$ GPa for **1-op** and $K = 1.40$ GPa for **2-op**), which reflects the exceptionally high flexibility and compressibility of the **op** phases of both materials. These values are even lower than the bulk modulus reported for the highly flexible large pore phase of MIL-53(Cr) ($K \sim 1.8$–2.0 GPa (ref. 28 and 42)) and also lower than previously reported for **1** ($K = 2.6$ GPa, determined from HP-PXRD data;[32] $K = 2.41$ GPa, determined via ab initio calculations[43]). The bulk moduli of the contracted **cp** phases are considerably larger ($K = 4.88$ GPa for **1-cp** and $K = 3.31$ GPa for **2-cp**), which arises due to their higher densities and very low porosities.

Since both ZIF-4(M) materials are isostructural, the different properties of their metal cations (Zn^{2+} vs. Co^{2+}) must account for their different high pressure behaviour. The ionic radii of tetrahedrally coordinated Zn^{2+} and Co^{2+} are very similar (Shannon radii:[44] 0.74 Å for Zn^{2+} and 0.72 Å for Co^{2+}), which results in almost identical unit cell parameters and unit cell volumes of their **op** phases (see Table 1). However, both metal ions feature markedly different electronegativities[45] (1.65 for Zn and 1.88 for Co) and specific electron configurations (3d^{10} for Zn^{2+} vs. 3d^7 for Co^{2+}). We hypothesise that the bonding of the im$^-$ linkers to the Zn^{2+} centres of compound **1** can solely be described by σ-bonding, while the 3d^7 electron configuration of Co^{2+} strongly suggests the presence of additional ligand-to-metal π-bonding for compound **2**. The π-bonding in **2** results qualitatively in stronger imidazolate–metal bonds compared to **1**, where π-bonding is absent. Furthermore, the higher electronegativity of Co suggests more covalent (directional) ligand-to-metal bonding for **2**, while in **1** these bonds are more ionic (non-directional) as a consequence of the lower electronegativity of Zn.

The pressure dependent phase behaviour of **1** and **2** directly reflects these fundamental chemical differences between their respective metal ions. It is evident that the phase transition from the **op** to the **cp** phase is associated with very significant distortions of the MN$_4$ tetrahedra and the M–im–M bonding angles (see ESI, Tables S1 and S2†). As a consequence of the more covalent and directional ligand-to-metal bonds, a higher mechanical pressure (~50 MPa) is needed to initiate the **op–cp** phase transition in **2**, while compound **1** requires a much lower pressure (~28 MPa). Advanced density functional theory calculations could shed light on the influence of the ligand-to-metal bonding on the high pressure phase behaviour of these compounds. These complex calculations (open shell nature of the 3d^7 Co^{2+} system), however, are beyond the scope of this work.

Nonetheless, the irreversibility of the **op–cp** transition of **1** in the mercury intrusion experiment (maximum pressure ~210 MPa) is surprising, because it was found that the **op** phase is entropically favoured over the **cp** phase at ambient temperature and pressure.[37] To verify the results from the mercury intrusion experiments, we performed an additional *ex situ* pressurisation experiment. A finely ground powder of freshly evacuated **1** was pelletized in a conventional pellet press (see ESI† for details) using a uniaxial pressure of ~190 MPa for about 10 min. After pressure release the obtained pellet was finely ground again and the material analysed by PXRD. The majority of the peaks in the diffraction pattern of pelletized **1** can be assigned to the **cp** phase, while some material remains in the **op** phase (Fig. S14†). We ascribe this to pressure inhomogeneities in the simple pelletizing experiment (uniaxial compression) compared to the previous mercury intrusion and HP-PXRD studies (hydrostatic compression). Notably, most of the contracted **cp** phase of the pelletized sample can be returned to the **op** phase by heating the sample to 130 °C for 8 h under vacuum. This finding strongly suggests that the **op–cp** phase transition is also reversible for **1**, but returning to the **op** phase requires a significant energy barrier to be overcome.

In fact, the inverse **cp–op** transition of **2** also involves a large energy barrier which gives rise to the very large hysteresis (width ~46 MPa) in the mercury intrusion experiment. Hence, we postulate that the lack of the **cp–op** transition upon decompression of **1** at ambient temperature originates from a similarly large pressure hysteresis. Thus, the **cp** phase of **1** is kinetically trapped after decompression at ambient temperature. However, the fact that the **op** phase of **1** can be recovered by heating the material to 130 °C clearly evidences that this phase is thermodynamically favoured over the **cp** phase at ambient pressure. For thermodynamic reasons (Clausius–Clapeyron relation), the threshold pressures for the **op–cp** transition (as well as for the reverse **cp–op** transition) will shift to lower values if the temperature is decreased or to higher values if the temperature is increased. Hence, if the mercury intrusion experiments could be done at 130 °C the **op–cp** transition should be directly reversible for compound **1** as well.

The strong influence of the metal cation on the material's mechanical phase behaviour suggests various chemical ways for a systematic fine-tuning of these properties. In the future, solid solution compounds containing both metal ions (Zn^{2+} and Co^{2+}) in varying ratios or even other dopant cations, such as Fe^{2+}, should be investigated.[1,46–49] Moreover, we anticipate that these ZIFs, as well as the related MIL-53/MIL-47 materials, could be very interesting materials for applications in mechanocalorics. We demonstrated that the molar entropy change, ΔS_m, for the low temperature **op–cp** phase transition of **1** amounts to about 60 J K^{-1} mol^{-1}.[37] If we assume a similar ΔS for the pressure-driven **op–cp** transition, a gravimetric ΔS_g of approx. 300 J K^{-1} kg^{-1} can be expected. This value is very high, even in comparison to current benchmark materials in the field of mechanocalorics (ΔS_g ~100–150 J K^{-1} kg^{-1}).[19] In future studies we aim to investigate the mechanocaloric properties of these materials in detail.

Conclusions

Our findings add the first group of ZIF materials to the small family of highly flexible MOFs that show breathing phase transitions under a stimulus of mechanical pressure. Open pore to closed pore phase transitions with a contraction of about 19–21% of the crystal volume are apparent for ZIF-4(Zn) and ZIF-4(Co). The metal ion, and thus the nature of ligand-to-metal bonding, plays a crucial role, not only for the phase transition pressure, but also for the immediate reversibility and repeatability of the process. For ZIF-4(Co), the transition is directly reversible upon decompression (at least if $p_{max} \leq 210$ MPa), while the phase transition is irreversible upon decompression for ZIF-4(Zn) but can be reversed *via* heating the material to 130 °C. This discovery proposes novel applications of these microporous ZIFs as shock absorbers (ZIF-4(Zn); irreversible transition) and nanodampers or in mechanocalorics (ZIF-4(Co); reversible transition). Our results further suggest there may exist similar breathing phase transitions in other ZIFs – a property so far mainly demonstrated by carboxylate-based MOFs.

Conflicts of interest

There are no conflicts to declare.

Acknowledgements

Notes and references

¶ In the MOF literature, the term breathing has not only been used for phase transitions that result in large changes of accessible pore volume upon gas or guest adsorption, but also for related transitions triggered by other stimuli, such as temperature or mechanical pressure. The term breathing is used here to underline the huge differences in unit cell volume (density) and accessible pore space between the two involved phases.

‖ We use the extended Hermann–Mauguin Symbols here to illustrate the relationship between the monoclinic settings and the original orthorhombic setting (space group *Pbca*). The unconventional monoclinic settings $P2_1/b11$ and $P112_1/a$ can be converted to the standard setting $P2_1/c$ (extended symbol $P112_1/c1$) by permuting the crystallographic axes (see ESI† for details).

** Obviously, W_{trans} depends on the actual phase transition pressure. The phase transition pressure, however, varies as a function of the utilised pressure transmitting fluid. In the following discussion, we only compare values of W_{trans}, which have been determined on the basis of mercury intrusion data, to ensure their direct comparability.

1 A. Schneemann, V. Bon, I. Schwedler, I. Senkovska, S. Kaskel and R. A. Fischer, *Chem. Soc. Rev.*, 2014, **43**, 6062.

2 S. Horike, S. Shimomura and S. Kitagawa, *Nat. Chem.*, 2009, **1**, 695.

3 G. Férey and C. Serre, *Chem. Soc. Rev.*, 2009, **38**, 1380.

4 Z. Chang, D. H. Yang, J. Xu, T. L. Hu and X. H. Bu, *Adv. Mater.*, 2015, **27**, 5432.

5 C. Serre, F. Millange, C. Thouvenot, M. Noguès, G. Marsolier, D. Louër and G. Férey, *J. Am. Chem. Soc.*, 2002, **124**, 13519.

6 C. Serre, S. Bourrelly, A. Vimont, N. A. Ramsahye, G. Maurin, P. L. Llewellyn, M. Daturi, Y. Filinchuk, O. Leynaud, P. Barnes and G. Férey, *Adv. Mater.*, 2007, **19**, 2246.

7 A. M. Walker, B. Civalleri, B. Slater, C. Mellot-Draznieks, F. Cora, C. M. Zicovich-Wilson, G. Roman-Perez, J. M. Soler and J. D. Gale, *Angew. Chem., Int. Ed.*, 2010, **49**, 7501.

8 F. Millange, N. Guillou, R. I. Walton, J.-M. Grenèche, I. Margiolaki and G. Férey, *Chem. Commun.*, 2008, 4732.

9 P. Serra-Crespo, E. Stavitski, F. Kapteijn and J. Gascon, *RSC Adv.*, 2012, **2**, 5051.

10 K. J. Gagnon, C. M. Beavers and A. Clearfield, *J. Am. Chem. Soc.*, 2013, **135**, 1252.

11 P. Serra-Crespo, A. Dikhtiarenko, E. Stavitski, J. Juan-Alcañiz, F. Kapteijn, F.-X. Coudert and J. Gascon, *CrystEngComm*, 2015, **17**, 276.

12 J. Im, N. Yim, J. Kim, T. Vogt and Y. Lee, *J. Am. Chem. Soc.*, 2016, **138**, 11477.

13 S. A. Moggach, T. D. Bennett and A. K. Cheetham, *Angew. Chem., Int. Ed.*, 2009, **48**, 7087.

14 A. J. Graham, D. R. Allan, A. Muszkiewicz, C. A. Morrison and S. A. Moggach, *Angew. Chem., Int. Ed.*, 2011, **50**, 11138.

15 A. J. Graham, J. C. Tan, D. R. Allan and S. A. Moggach, *Chem. Commun.*, 2012, **48**, 1535.

16 A. J. Graham, A. M. Banu, T. Duren, A. Greenaway, S. C. McKellar, J. P. Mowat, K. Ward, P. A. Wright and S. A. Moggach, *J. Am. Chem. Soc.*, 2014, **136**, 8606.

17 S. C. McKellar, A. J. Graham, D. R. Allan, M. I. Mohideen, R. E. Morris and S. A. Moggach, *Nanoscale*, 2014, **6**, 4163.

18 A. Kitanovski, U. Plaznik, U. Tomc and A. Poredoš, *Int. J. Refrig.*, 2015, **57**, 288.

19 L. Manosa and A. Planes, *Adv. Mater.*, 2017, **29**, 1603607.

20 I. Beurroies, M. Boulhout, P. L. Llewellyn, B. Kuchta, G. Férey, C. Serre and R. Denoyel, *Angew. Chem., Int. Ed.*, 2010, **49**, 7526.

21 P. G. Yot, Q. Ma, J. Haines, Q. Yang, A. Ghoufi, T. Devic, C. Serre, V. Dmitriev, G. Férey, C. Zhong and G. Maurin, *Chem. Sci.*, 2012, **3**, 1100.

22 P. G. Yot, Z. Boudene, J. Macia, D. Granier, L. Vanduyfhuys, T. Verstraelen, V. Van Speybroeck, T. Devic, C. Serre, G. Ferey, N. Stock and G. Maurin, *Chem. Commun.*, 2014, **50**, 9462.

23 J. Rodriguez, I. Beurroies, T. Loiseau, R. Denoyel and P. L. Llewellyn, *Angew. Chem., Int. Ed.*, 2015, **54**, 4626.

24 P. G. Yot, L. Vanduyfhuys, E. Alvarez, J. Rodriguez, J.-P. Itié, P. Fabry, N. Guillou, T. Devic, I. Beurroies, P. L. Llewellyn, V. Van Speybroeck, C. Serre and G. Maurin, *Chem. Sci.*, 2016, **7**, 446.

25 P. Ramaswamy, J. Wieme, E. Alvarez, L. Vanduyfhuys, J.-P. Itié, P. Fabry, V. Van Speybroeck, C. Serre, P. G. Yot and G. Maurin, *J. Mater. Chem. A*, 2017, **5**, 11047.

26 J. Rodriguez, I. Beurroies, M. V. Coulet, P. Fabry, T. Devic, C. Serre, R. Denoyel and P. L. Llewellyn, *Dalton Trans.*, 2016, **45**, 4274.

27 P. G. Yot, K. Yang, V. Guillerm, F. Ragon, V. Dmitriev, P. Parisiades, E. Elkaïm, T. Devic, P. Horcajada, C. Serre, N. Stock, J. P. S. Mowat, P. A. Wright, G. Férey and G. Maurin, *Eur. J. Inorg. Chem.*, 2016, **2016**, 4424.

28 A. V. Neimark, F.-X. Coudert, C. Triguero, A. Boutin, A. H. Fuchs, I. Beurroies and R. Denoyel, *Langmuir*, 2011, **27**, 4734.

29 Y. Q. Tian, Y. M. Zhao, Z. X. Chen, G. N. Zhang, L. H. Weng and D. Y. Zhao, *Chem.–Eur. J.*, 2007, **13**, 4146.

30 K. S. Park, Z. Ni, A. P. Cote, J. Y. Choi, R. Huang, F. J. Uribe-Romo, H. K. Chae, M. O'Keeffe and O. M. Yaghi, *Proc. Natl. Acad. Sci. U. S. A.*, 2006, **103**, 10186.

31 T. D. Bennett, A. L. Goodwin, M. T. Dove, D. A. Keen, M. G. Tucker, E. R. Barney, A. K. Soper, E. G. Bithell, J. C. Tan and A. K. Cheetham, *Phys. Rev. Lett.*, 2010, **104**, 115503.

32 T. D. Bennett, P. Simoncic, S. A. Moggach, F. Gozzo, P. Macchi, D. A. Keen, J. C. Tan and A. K. Cheetham, *Chem. Commun.*, 2011, **47**, 7983.

33 T. D. Bennett, J. C. Tan, Y. Yue, E. Baxter, C. Ducati, N. J. Terrill, H. H. Yeung, Z. Zhou, W. Chen, S. Henke, A. K. Cheetham and G. N. Greaves, *Nat. Commun.*, 2015, **6**, 8079.

34 T. D. Bennett, S. Cao, J. C. Tan, D. A. Keen, E. G. Bithell, P. J. Beldon, T. Friscic and A. K. Cheetham, *J. Am. Chem. Soc.*, 2011, **133**, 14546.

35 M. R. Ryder and J. C. Tan, *Dalton Trans.*, 2016, **45**, 4154.

36 R. Gaillac, P. Pullumbi, K. A. Beyer, K. W. Chapman, D. A. Keen, T. D. Bennett and F. X. Coudert, *Nat. Mater.*, 2017, **16**, 1149.

37 M. T. Wharmby, S. Henke, T. D. Bennett, S. R. Bajpe, I. Schwedler, S. P. Thompson, F. Gozzo, P. Simoncic, C. Mellot-Draznieks, H. Tao, Y. Yue and A. K. Cheetham, *Angew. Chem., Int. Ed.*, 2015, **54**, 6447.

38 Y.-Q. Tian, Z.-X. Chen, L.-H. Weng, H.-B. Guo, S. Gao and D. Y. Zhao, *Inorg. Chem.*, 2004, **43**, 4631.

39 G. S. Pawley, *J. Appl. Crystallogr.*, 1981, **14**, 357.

40 B. Fultz, *Prog. Mater. Sci.*, 2010, **55**, 247.

41 H. Giesche, *Part. Part. Syst. Charact.*, 2006, **23**, 9.

42 Q. Ma, Q. Yang, A. Ghoufi, G. Férey, C. Zhong and G. Maurin, *Dalton Trans.*, 2012, **41**, 3915.

43 J.-C. Tan, B. Civalleri, A. Erba and E. Albanese, *CrystEngComm*, 2015, **17**, 375.

44 R. D. Shannon, *Acta Crystallogr., Sect. A: Cryst. Phys., Diffr., Theor. Gen. Crystallogr.*, 1976, **32**, 751.

45 A. L. Allred, *J. Inorg. Nucl. Chem.*, 1961, **17**, 215.

46 I. Schwedler, S. Henke, M. T. Wharmby, S. R. Bajpe, A. K. Cheetham and R. A. Fischer, *Dalton Trans.*, 2016, **45**, 4230.

47 F. Nouar, T. Devic, H. Chevreau, N. Guillou, E. Gibson, G. Clet, M. Daturi, A. Vimont, J. M. Greneche, M. I. Breeze, R. I. Walton, P. L. Llewellyn and C. Serre, *Chem. Commun.*, 2012, **48**, 10237.

48 H. Deng, C. J. Doonan, H. Furukawa, R. B. Ferreira, J. Towne, C. B. Knobler, B. Wang and O. M. Yaghi, *Science*, 2010, **327**, 846.

49 H. Zhang, S. Hwang, M. Wang, Z. Feng, S. Karakalos, L. Luo, Z. Qiao, X. Xie, C. Wang, D. Su, Y. Shao and G. Wu, *J. Am. Chem. Soc.*, 2017, **139**, 14143.